



# Combined Doxorubicin Mesoporous Carbon Nanospheres for Effective Tumor Lymphatic Metastasis by Multi-Modal Chemo-Photothermal Treatment in vivo

Yipengchen Yin <sup>1,\*</sup>, Jiaxin Sun<sup>2,\*</sup>, Tiaoyan Jiang<sup>1</sup>, Li Zhu<sup>3</sup>, Wenchao Gu<sup>4</sup>, Sheng Wang<sup>5</sup>, Le Song<sup>6</sup>, Changchun Wang<sup>2</sup>, Qin Zhang <sup>1</sup>

<sup>1</sup>Department of Radiation Oncology, Shanghai Chest Hospital, Shanghai Jiao Tong University School of Medicine, Shanghai, 200030, People's Republic of China; <sup>2</sup>State Key Laboratory of Molecular Engineering of Polymers, Department of Macromolecular Science, and Laboratory of Advanced Materials, Fudan University, Shanghai, 200438, People's Republic of China; <sup>3</sup>Department of Radiology, Shanghai Chest Hospital, Shanghai Jiao Tong University School of Medicine, Shanghai, 200030, People's Republic of China; <sup>4</sup>Department of Diagnostic and Interventional Radiology, University of Tsukuba, Ibaraki, 305-8575, Japan; <sup>5</sup>Department of Colorectal Surgery, Fudan University Shanghai Cancer Center, Shanghai, 200032, People's Republic of China; <sup>6</sup>Department of Gerontology, Zhongshan Hospital, Fudan University, Shanghai, 200032, People's Republic of China

\*These authors contributed equally to this work

Correspondence: Qin Zhang; Le Song, Email zhangqin@shsmu.edu.cn; song.le@zs-hospital.sh.cn

**Introduction:** Sentinel lymph node (SLN) is the first regional lymph node where tumor cells metastasize, and its identification and treatment are of great significance for the prevention of tumor metastasis. However, the current clinical modalities for identification and treatment of SLN are still far from satisfactory owing to their high cost, invasiveness and low accuracy. We aim to design a novel nanomedicine system for SLN imaging and treatment with high efficacy.

**Methods:** We designed and prepared hollow mesoporous carbon spheres (HMCS) and loaded with the chemotherapeutic drug doxorubicin (DOX), which is then modified with polyvinyl pyrrolidone (PVP) to obtain nanomedicine: HMCS-PVP-DOX.

**Results:** HMCS-PVP with a size of about 150 nm could retain in the lymph nodes for a long time and stain the lymph nodes, which could be easily observed by the naked eye. At the same time, HMCS-PVP exhibited excellent photoacoustic and photothermal imaging capabilities, realizing multimodal imaging to locate lymph nodes precisely. Due to its high specific surface area, HMCS could be largely loaded with the chemotherapeutic drug doxorubicin (DOX). HMCS-PVP-DOX displayed highly efficient synergistic chemotherapy-photothermal therapy for lymphatic metastases in both cellular and animal experiments due to its significant photothermal effect under 1064 nm laser irradiation. HMCS-PVP-DOX also displayed great stability and biosafety.

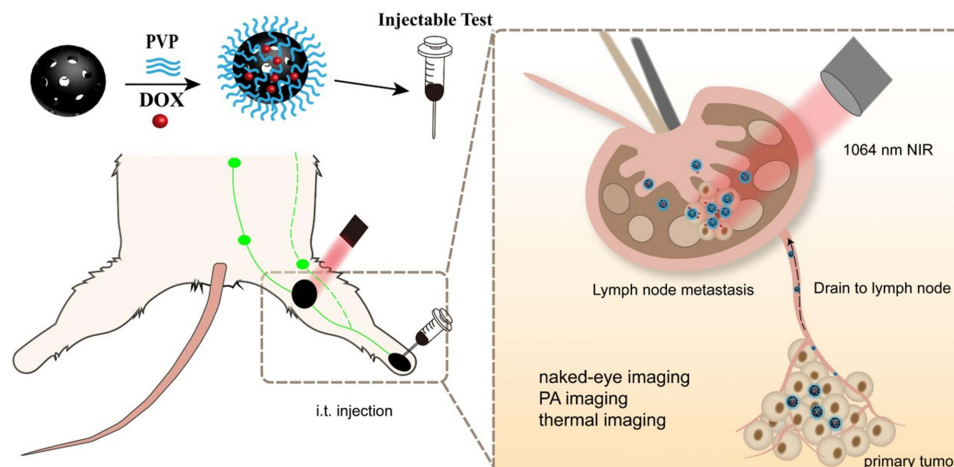
**Discussion:** Multifunctional nanomedicine HMCS-PVP-DOX is expected to provide a novel paradigm for designing nanomedicine to the diagnosis and treatment of lymphatic metastases because of its good stability and safety.

**Keywords:** tumor lymphatic metastasis theranostics, hollow mesoporous carbon nanospheres, sentinel lymph node, tri-modal imaging, chemo-photothermal therapy

## Introduction

Cancer has one of the highest worldwide mortality indices of any disease.<sup>1</sup> Approximately 90% of cancer mortalities are due to tumor metastasis rather than primary tumor growth.<sup>2,3</sup> Tumor metastasis comprises four consecutive steps: (1) Cancer cells detach from the original tumor mass and become aggressive; (2) Enter the circulation via blood or lymphatic vessels; (3) Extravasate and spread to distant organs to form the micrometastasis; (4) Finally outgrow into macroscopic metastasis.<sup>4</sup> The lymphatic system plays a pivotal role in tumor metastasis.<sup>5,6</sup> Sentinel lymph node (SLN) – the first lymph node that receives lymphatic drainage from a tumor – is also theoretically the first to receive metastatic seeding.<sup>7</sup>

## Graphical Abstract



If the SLN is negative for metastasis, the chance of metastases in other lymph nodes is very slim, then no further surgery will be performed.<sup>8,9</sup> Sentinel lymph node biopsy (SLNB) is a standard approach for axillary lymph node status evaluation in clinically node-negative breast cancer patients.<sup>10</sup> The accuracy of SLNB is 95% for extremely proficient clinicians, which is extensively dependent on the experience of surgeons.<sup>11</sup> X-ray computed tomography (CT),<sup>12</sup> magnetic resonance imaging (MRI),<sup>13</sup> positron emission tomography (PET),<sup>14</sup> single-photon emission computed tomography (SPECT)<sup>15</sup> and fluorescence imaging (FL)<sup>16</sup> are current medical imaging techniques, which yield images with high spatial resolution. Unfortunately, exposure to radiation and high costs of equipment and reagents hamper their widespread applications in clinical practice.<sup>17,18</sup> As an alternative to optical methods, photoacoustic (PA) imaging is emerging as one of the most efficient diagnostic strategies for real-time noninvasive monitoring of SLN.<sup>19</sup> Compared with invasive diagnostic tools, which augment the jeopardy of nerve damage, hematoma and lymphedema formation, nanomaterial-based exogenous contrast agents and PA imaging propose a novel strategy for non-invasive, non-radiative and high-resolution SLN mapping.<sup>20–22</sup>

Carbon nanomaterials, for instance, carbon nanodot, carbon nanotube and bioink are effortlessly distinguished from living organisms by the naked eye in virtue of their black color.<sup>23–26</sup> Carbon nanoparticles suspension injection is a clinically utilized lymphatic contrast agent. However, the preparation of these carbon materials for clinical lymphatic tracer is cumbersome and costly. It is exceedingly momentous to scheme an economical and efficacious lymphatic tracer for clinical implementation.<sup>27</sup> Moreover, the matching of the surgical window and the migration and distribution of nanoparticles are crucial to clinical manipulation. The size of the nanoparticles is the pivotal facet in governing the interstitium diffusion rate, lymphatic drainage and uptake of lymph nodes. The diameter of the capillaries is nigh 30–50 nm, and the lymphatic capillary endothelial cells are aligned in shingles with a gap of 120–500 nm. If the diameter of the nanoparticles is greater than 100 nm, they can merely enter the lymphatic vessels instead of capillaries. Regional lymph node dissection guided by staining visible to the naked eye remains the sole clinical treatment for lymphatic metastases.<sup>28</sup> Photothermal therapy (PTT) proves to be one of the most paramount treatment modalities for tumor models attributable to its less invasiveness and higher biosafety.<sup>29,30</sup> At this juncture, there retain few studies on PTT for lymph node metastasis models.<sup>31</sup> Imaging-guided PTT can be exploited to eradicate lymph nodes with latent metastases, which has implications for the clinical transformation.

Inspired by the relationship between the size of nanoparticles and the targeting ability of lymphatic vessels, we designed and prepared a tri-modal imaging (naked-eye recognition/PA imaging/photothermal imaging) platform, hollow mesoporous carbon nanospheres-polyvinyl pyrrolidone-doxorubicin (HMCS-PVP-DOX), to medicate lymph node

metastasis models. The size of HMCS-PVP-DOX was apposite to selectively accumulate in the SLN, and DOX exhibit chemotherapeutic effectuality against lymphatic metastases. HMCS-PVP-DOX showed splendid fluorescence detection, marvelous visual and PA observation idiosyncrasies in both normal and metastatic SLN, which was germane for the location and treatment of SLN metastases with satisfactory biological safety.

## Materials and Methods

### Preparation of Hollow Mesoporous Carbon Nanospheres-Polyvinyl Pyrrolidone (HMCS-PVP)

A 3 mL of ammonia solution ( $\text{NH}_3 \cdot \text{H}_2\text{O}$ , 25%wt), 20 mg of DI water and 47 mg of ethanol were mixed and stirred under magnetic stirring at  $30^\circ\text{C}$  for 15 min. Subsequently, 2 mL of TPOS, 0.4 g of resorcinol and 0.56 mL of formaldehyde were added to the reaction solution and the reaction was continued for 12 h. The crude product  $\text{SiO}_2@\text{SiO}_2/\text{RF}$  was purified by centrifugation (10,000 rpm, 5 min) using ethanol and water alternately three times and the crude product was dried in an oven at  $80^\circ\text{C}$  overnight. Then,  $\text{SiO}_2@\text{SiO}_2/\text{RF}$  was synthesized as the intermediate product  $\text{SiO}_2@\text{SiO}_2/\text{C}$  by increasing the temperature to  $800^\circ\text{C}$  in a nitrogen stream at a ramp rate of  $5^\circ\text{C}$  and maintaining it for 3 h. Finally, the silica was removed from  $\text{SiO}_2@\text{SiO}_2/\text{C}$  with aqueous NaOH (2 M) under magnetic stirring in an oil bath at  $90^\circ\text{C}$ . Hollow mesoporous carbon nanoparticles were obtained after washing with water and ethanol alternately for three times, after which HMCS was obtained by drying.

HMCS and PVP were mixed by shaking in PBS at a mass ratio of 1:1 and sonicated for 30 min to prepare an equivalent concentration of  $50\text{ mg mL}^{-1}$  of HMCS. Then, centrifugation was performed at 15,000 rpm for 20 min to remove the free PVP. After modification, the injectability of HMCS-PVP was tested by taking a 1 mL syringe and aspirating the injected sample.

### Lymphatic Imaging Capability of Hollow Mesoporous Carbon Nanospheres-Polyvinyl Pyrrolidone (HMCS-PVP)

A  $50\ \mu\text{L}$  of HMCS-PVP suspension ( $50\text{ mg mL}^{-1}$ ) was injected into the foot pads of BALB/c female mice, and the mice were executed at 30 min, 60 min, 120 min and 24 h. The skin at the popliteal region of the leg was cut open and the staining of the anterior lymph nodes was observed visually and photographed with a digital camera.

### The Photothermal Effect of Hollow Mesoporous Carbon Nanospheres-Polyvinyl Pyrrolidone (HMCS-PVP)

A  $100\ \mu\text{L}$  of HMCS-PVP at different concentrations (25, 50,  $100\ \mu\text{g mL}^{-1}$ ) was irradiated with NIR laser ( $1064\text{ nm}$ ,  $1\text{ W cm}^{-2}$ , 5 min), and the temperature of the solution was recorded every 10 seconds with a thermal infrared imager. Afterwards, the laser was turned off and the temperature of the samples was recorded with the thermal infrared imager as they cooled down under natural conditions until the temperature dropped to room temperature. In addition, the absorbance at 700–1300 nm of HMCS-PVP suspensions at different concentrations was tested with UV spectrophotometer and the photothermal conversion efficiency of HMCS-PVP was calculated.

### Loading and Release of Doxorubicin

DOX was mixed with HMCS-PVP at a mass ratio of 1:9 and sonicated for 15 min in PBS to obtain HMCS-PVP-DOX. After that, HMCS-PVP-DOX was dialyzed in different pH buffers (pH=5.5 or 7.4), and 5 mL of the solution was removed to test UV absorbance per minute. To explore the influence of NIR irradiation on drug release, the solution (pH=5.5 or 7.4) was exposed to  $1064\text{ nm}$  laser ( $1\text{ W cm}^{-2}$ ) for 5 min and UV absorbance was tested per minute. The loading and release efficiency of HMCS-PVP-DOX was calculated.

### In vitro Experiments

Mouse breast cancer cells (4T1) and human embryonic kidney cells (HEK-293) were purchased from Wuhan Procell Life Science & Technology Co., Ltd. (Wuhan, China). To investigate the biosafety of HMCS-PVP and HMCS-PVP-DOX,

CCK-8 test was performed. First, 4T1 cells and HEK-293 cells were inoculated into 96-well plates at a density of 10,000 cells per well, and then incubated for 24 h until the cells were plastered, after which the medium was aspirated and incubated for 24 h with a medium solution of HMCS-PVP, HMCS-PVP-DOX or DOX, after which the medium was aspirated and a medium solution of CCK-8 was added, and the cell viabilities were measured by CCK-8 kit.

To explore the effect of HMCS-PVP-DOX on cell viabilities, cells were inoculated into 96-well plates at a density of 10,000 cells per well, and then incubated for 24 h until the cells were plastered, after which the medium was aspirated and incubated for 4 h with a medium solution of HMCS-PVP or HMCS-PVP-DOX, followed by NIR laser (1064 nm, 1 W cm<sup>-2</sup>) irradiation for 5 min and incubation for 24 h. Cell viabilities of 4T1 cells were determined with CCK-8 kit.

## In vivo Experiments

### Establishment of Mouse Model of Lymphatic Metastasis Tumor

The BALB/c female mice (6–8 weeks) were purchased from Shanghai Slac Laboratory Animal Co. Ltd. (Shanghai, China) and housed in clean room. All animal experiments were approved by the Animal Experiment Ethics Committee of Fudan University (2014–03-YJ-PZQ-01) and were complied with the Animal Management Rules issued by the Ministry of Health of the People's Republic of China (Document No. 55, 2001). The mice were injected with 4T1 cells (100  $\mu$ L, about  $3 \times 10^6$  cells in PBS dispersion) into the left foot pad at 5 weeks, and the lymph nodes metastases were successfully established after 1 week, followed by tumor treatment and imaging experiments.<sup>32</sup>

### Photoacoustic (PA)/Photothermal Imaging Studies

For in vitro PA imaging, a high-resolution PA imaging system was used to test the PA signal of various concentrations of HMCS-PVP-DOX. For in vivo PA imaging, the leg hair on the seed tumor side was removed from the mice using hair removal cream, and then the foot pads of 4T1 tumor-bearing mice were injected with HMCS-PVP-DOX to test the PA signal at the lymphatic metastasis site.

The optimal time for HMCS-PVP-DOX enrichment was identified by PA imaging, and then mice were anesthetized and irradiated with a NIR laser (1064 nm, 0.75 W cm<sup>-2</sup>) for 5 min. The temperature at lymphatic metastases tumors per minute was recorded with a thermal infrared imager.

### In vivo Cancer Therapy

Lymphatic metastases mice were randomly divided into 6 groups (n=5): PBS group (control group), DOX group, HMCS-PVP group, HMCS-PVP-DOX group, HMCS-PVP+Laser group and HMCS-PVP-DOX+Laser group. A 50  $\mu$ L solution (HMCS=50 mg mL<sup>-1</sup> or free DOX=5 mg mL<sup>-1</sup>) was injected into each mouse foot pads. One hour later, the tumor site was irradiated with 1064 nm NIR laser (0.75 W cm<sup>-2</sup>) for 5 min, and the temperature was recorded by thermal infrared imager. The body weight of the mice was recorded every two days. On day 16, all mice were dissected and their lymph node metastases tumors were collected and weighed, and the tumors and major organ tissues were stained with hematoxylin-eosin for histological analysis. To further evaluate the biosafety of HMCS-PVP and HMCS-PVP-DOX in vivo, 9 ICR mice were randomly divided into 3 groups, and the experimental group was injected HMCS-PVP or HMCS-PVP-DOX (50  $\mu$ L in PBS, HMCS=50 mg mL<sup>-1</sup>) via foot pads. Blood (2 mL) was collected 48 h after injection and was tested for blood routine and blood biochemical parameters with kits.

## Statistical Analysis

All results were expressed as mean  $\pm$  standard deviation (SD). Differences between individual experimental groups were analyzed using *t*-test.  $p < 0.05$  was considered to be statistically significantly different. \*Represents  $p < 0.05$ , \*\*Represents  $p < 0.01$ , and \*\*\*Represents  $p < 0.001$ .

## Results and Discussion

### Preparation and Characterization of HMCS-PVP-DOX

The migration of lymphatic tracer in the lymphatic vessels demanded appropriate hydrodynamic diameters, as small size contrast agents (<10 nm) were rapidly transported and diffused throughout the lymphatic vessels and lymph nodes;<sup>33,34</sup>

medium-sized contrast agents (50–200 nm) could be retained in the lymph nodes due to their slow rate of transport through the lymphatic vessels;<sup>35,36</sup> large size contrast agents (>500 nm) usually migrated through macrophages and dendritic cells in the lymphatic vessels, so the migration rate was very slow and might not even reach the lymph nodes.<sup>37</sup> The ideal tracer was one with right size not only to enter the lymphatic vessels without entering the capillaries, but to reach the SLN and remained there for a long time without reaching the distant lymph nodes prematurely, making it possible to directly determine the location of the SLN.

Based on the previously developed method,<sup>38</sup> we prepared HMCS with high photothermal conversion efficiency. In this experiment, we controlled the size of nanoparticles to about 150 nm by reducing the amount of silica precursor feeding. The results of TEM and FESEM (Figure 1) showed that the nanoparticles were relatively uniform in size with a hollow structure, and the shell layer had radial mesoporous pores. The size of the nanoparticles did not change significantly after modification and loading of drugs, providing an exploitable premise for their application in lymphatic imaging.

After that, nitrogen adsorption-desorption isotherm experiments (Figure 2a and b) were performed to examine the changes of specific surface area of carbon nanoparticles after modification with PVP and loading with DOX. The specific surface area of HMCS nanoparticles decreased from 605.0 cm<sup>2</sup> g<sup>-1</sup> to 286.2 cm<sup>2</sup> g<sup>-1</sup> after modification with PVP, and further decreased to 202.2 cm<sup>2</sup> g<sup>-1</sup> after loading with DOX. Both surface PVP and DOX had been successfully loaded. Raman spectroscopy (Figure 2d) showed that the surface modification of HMCS with PVP and DOX had no significant effect on its own graphite-like structure, which still has G-band (1598 cm<sup>-1</sup>) and D-band (1340 cm<sup>-1</sup>).

## Loading and Release of DOX

The loading of DOX was driven by the  $\pi$ - $\pi$  interaction between the two components, and it could be seen from the infrared results (Figure 2c) that DOX had been successfully loaded by HMCS-PVP. The appearance of 1575 cm<sup>-1</sup> and 1211 cm<sup>-1</sup> on the infrared spectrum were the absorption peaks of primary amine N-H bending vibration and hydroxyl O-H bending vibration, respectively, proving that DOX had been loaded onto the HMCS-PVP nanoparticles. By using the standard curve of Figure 3a, the encapsulation and loading rates of DOX could be calculated as 99.2% and 9.9%, respectively.

Figure 3b shows the drug release profile. The results showed that DOX was protonated in the acidic condition and became more soluble in the solution due to its hydrophilic nature, so it was facile to release from the carbon nanocarriers.

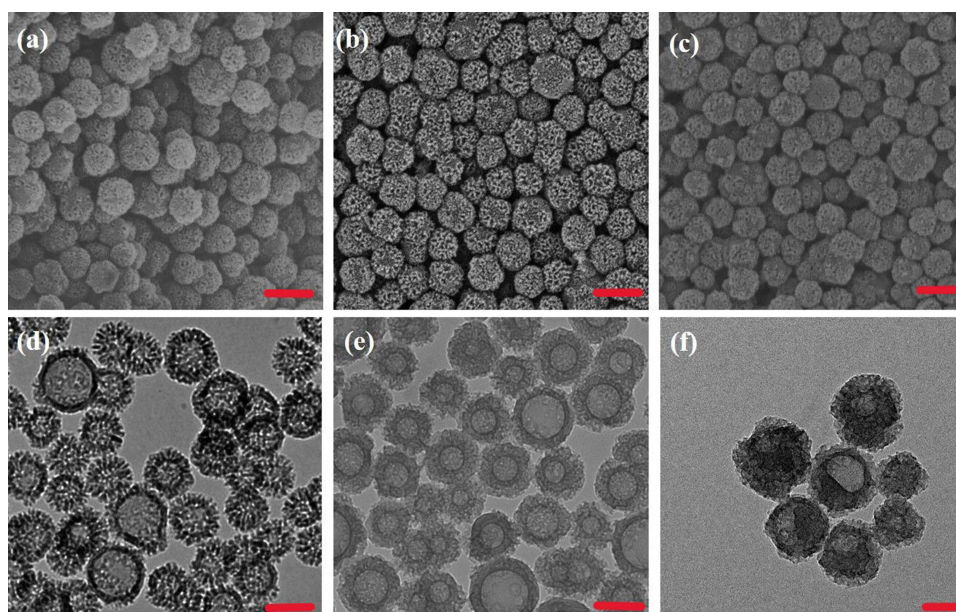


**Figure 1** FESEM images of (a) HMCS, (b) HMCS-PVP, (c) HMCS-PVP-DOX and TEM images of (d) HMCS, (e) HMCS-PVP, (f) HMCS-PVP-DOX. The scale bars in FESEM were 200nm, and the scale bars in TEM were 100 nm.

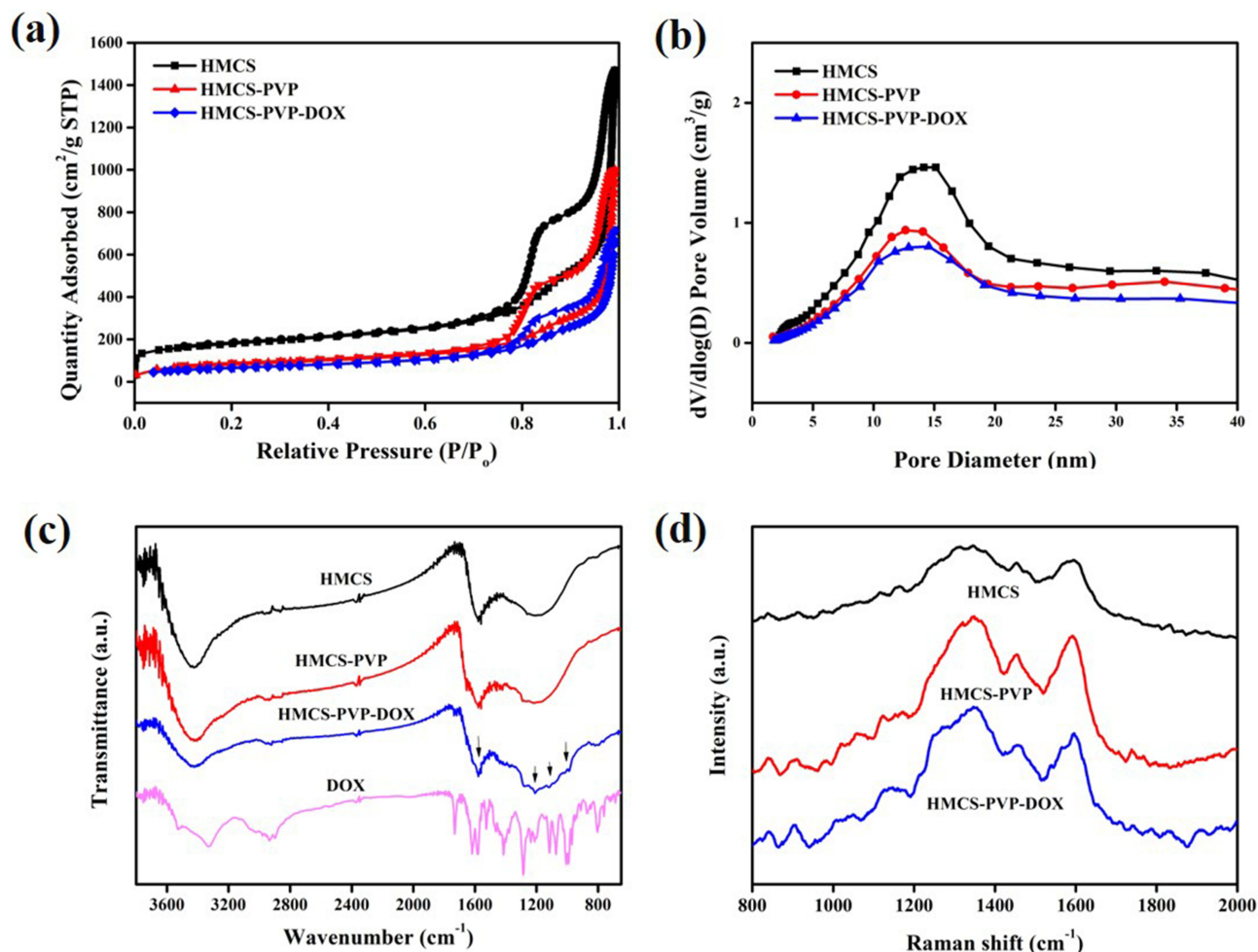


**Figure 2** (a) Nitrogen adsorption-desorption isotherms. (b) Pore volume distribution curves. (c) FT-IR spectra and (d) Raman spectra of HMCS, HMCS-PVP and HMCS-PVP-DOX.

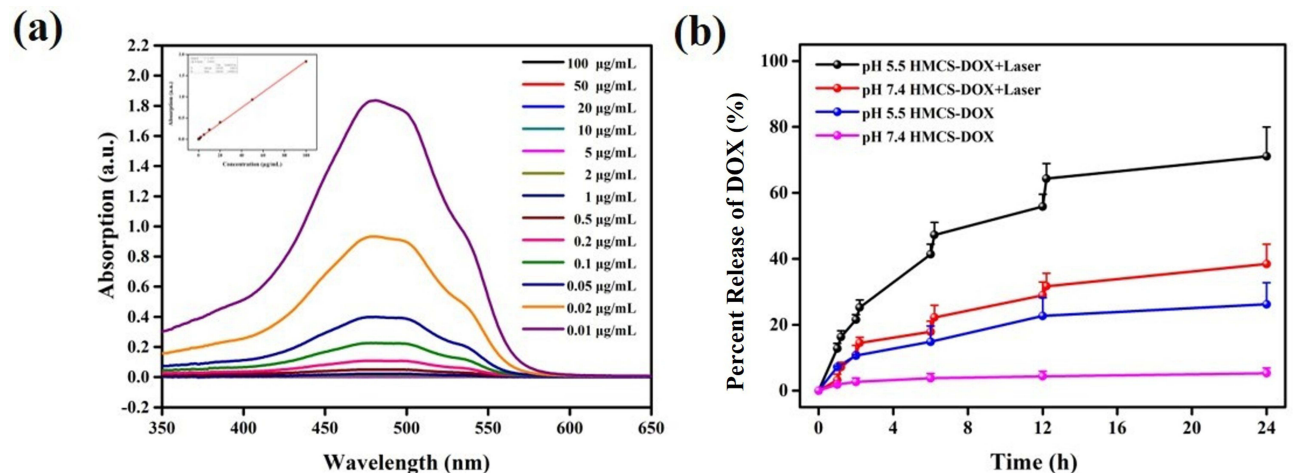


**Figure 3** (a) Standard curve of concentration-absorbance of DOX. (b) Controlled DOX release from HMCS-PVP-DOX after exposure to (1064 nm, 1 W cm<sup>-2</sup>) laser irradiation for 5 min in specific time period under different pH conditions.

The release of DOX could reach 71% under NIR laser irradiation and acidic condition, which was higher than 38% under the same acidic condition without laser irradiation, indicating that laser irradiation accelerated the thermal movement of drug molecules, which was conducive to the rapid release of DOX. The release of DOX was only 26% in the absence of laser irradiation at pH=7.4. Therefore, an additional laser could be used in the lymph nodes to promote the slow release of the drug to kill the tumor cells in the lymph nodes.

## Photothermal Effect of HMCS-PVP

According to the formula of photothermal conversion efficiency and ultraviolet (UV) absorbance (Figure 4), the photothermal conversion efficiency of HMCS-PVP under 1064 nm laser irradiation was 50.5%. HMCS could rise to 54.8 °C at a concentration of 25 µg mL<sup>-1</sup>, which was the temperature at which PTT was used to kill tumor cells. The photothermal effect of HMCS was correlated with the concentration of nanoparticles, the higher the concentrations of the nanoparticles, the higher the temperature rose, and this feature of nanoparticles could be used to adjust the photothermal effect by adjusting the enrichment of nanoparticles. It was known that the photothermal stability of carbon nanoparticles was very good, and the photothermal stability could be maintained even if repeated laser radiation was performed.

## Lymphatic Imaging

To examine the enrichment of HMCS-PVP at the lymph nodes and its effect as a naked-eye lymphatic tracer. Four BALB/c female mice were injected with HMCS-PVP suspension in the foot pad of each mouse, and then the mice were executed at different intervals and the skin of the leg curvature on the injection side was cut open (Figure 5). After 24 hours, the black stained lymph nodes could still be observed, indicating that the black staining effect of HMCS-PVP was obvious and could last up to 1 day with no attenuation of the obvious contrast.

To further test its ability to be located in lymph node imaging, the *in vitro* PA signal of HMCS-PVP nanoparticles was first examined. From Figure S1, HMCS-PVP showed a concentration-dependent linear relationship *in vitro*, indicating that HMCS-PVP was a potentially good contrast agent for PA imaging of lymph nodes. The maximum absorption wavelength of HMCS-PVP nanoparticles was 715 nm.

HMCS-PVP-DOX dispersion was injected into the foot pads of 4T1 lymphatic metastasis mice, and the anterior lymphatic metastasis sites of these mice were photographed with PA imaging at predetermined time points (0, 1, 2, 6, 12, 24, 48 h). The PA signal of the tumor was observed at different times using ultrasound (UA) imaging of the tumor tissue as a PA imaging background (Figure 6a). The results of the quantitative analysis of PA at the tumor site showed that the maximum enrichment of nanoparticles at the lymphatic tumor was 1 h after administration, and the intensity was maintained throughout (Figure 6b). The PA intensity of nanoparticles also remained high 48 h after injection. From the results, it was clear that after 1 h from the injection of the mouse footpad it could be used for photothermal therapy or

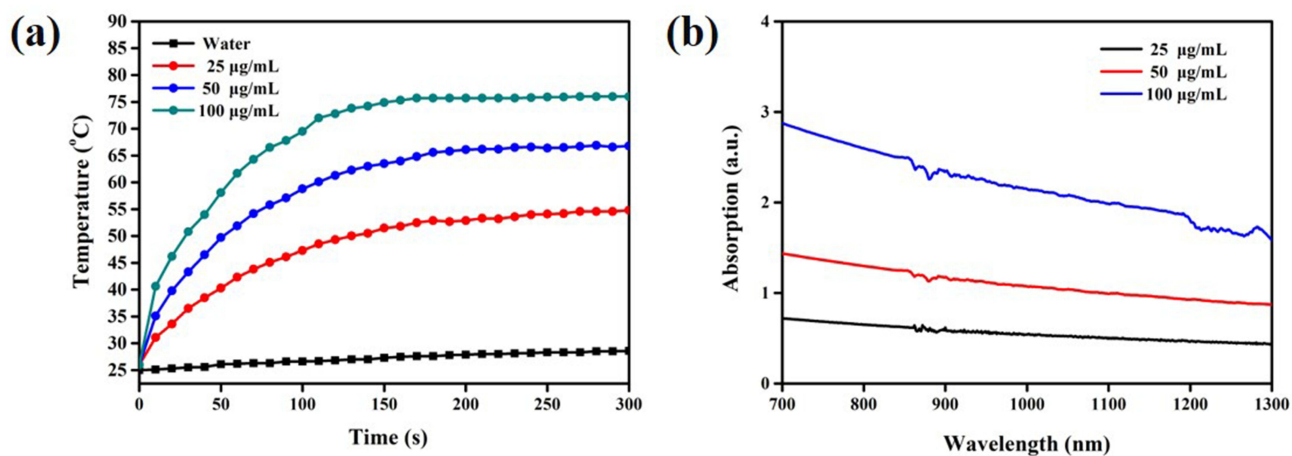


**Figure 4** (a) Photothermal performance of HMCS-PVP dispersion irradiated 1064 nm laser with different concentrations. (b) UV absorption of HMCS-PVP with different concentrations.

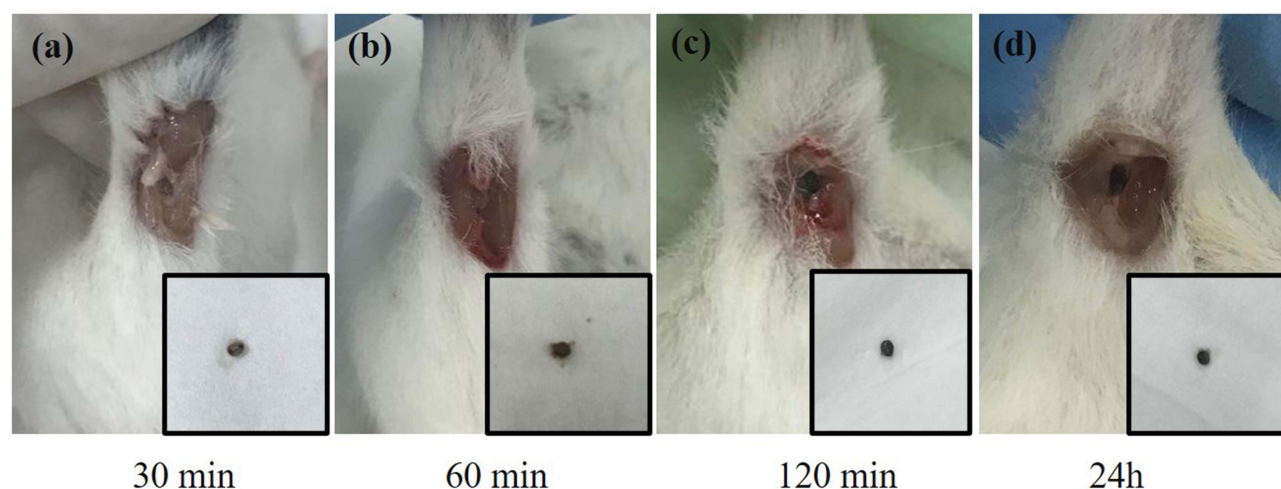


**Figure 5** Photos of sentinel lymph nodes at different times (a) 30 min, (b) 60 min, (c) 120 min, (d) 24 h after injection of HMCS-PVP in mouse footpad.

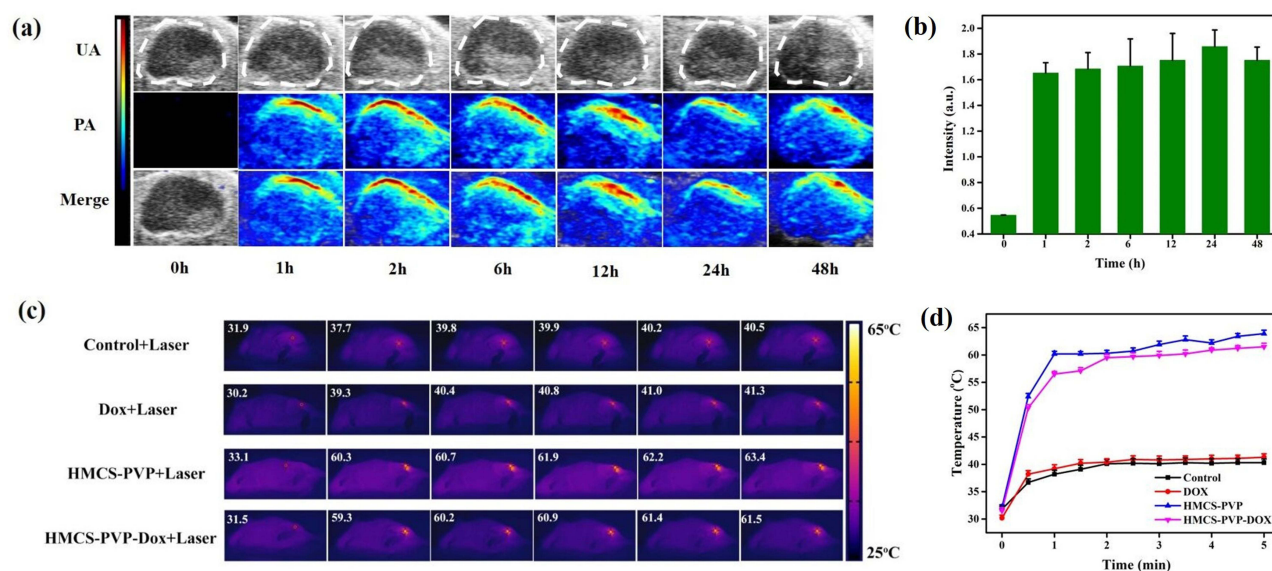


**Figure 6** (a) Ultrasonic imaging (UA)/photoacoustic (PA) images of lymph node metastasis. (b) PA signal intensity in lymph node metastasis varies with time post i.v. injection of HMCS-PVP-DOX. (c) Thermal images of 4T1 lymph node metastasis mice exposed to laser (1064 nm, 0.75W cm<sup>-2</sup>) irradiation for 5 min at 24h of footpad injection with different dispersions (PBS, DOX, HMCS-PVP and HMCS-PVP-DOX). (d) Temperature variation of 4T1 lymph node metastasis mice of different groups exposed to laser (1064 nm, 0.75W cm<sup>-2</sup>).

naked eye/PA observation, and the time of observation could be chosen over a long period of time, providing a less invasive and non-invasive way of observation for lymphography.

To investigate the feasibility of photothermal ablation of metastatic lymph nodes to replace the traditional surgical lymph node dissection approach, we performed laser treatment (1064 nm, 0.75 W cm<sup>-2</sup>, 5 min) on lymphatic metastases injected with HMCS-PVP in the footpad, and the lymph nodes of mice in the HMCS-PVP and HMCS-PVP-DOX groups could be elevated by 1 min of NIR irradiation to 63.9 °C and 61.5 °C within 1 min of NIR irradiation (Figure 6c and d), which was much higher than that of the control and DOX groups (40.3 °C and 41.3 °C), and the temperature reached the maximum within 1 min of irradiation and could be maintained until the end of laser irradiation, showing that HMCS-PVP had satisfactory photothermal properties, and HMCS-PVP nanoparticles loaded with DOX did not decay significantly due to the addition of the drug.



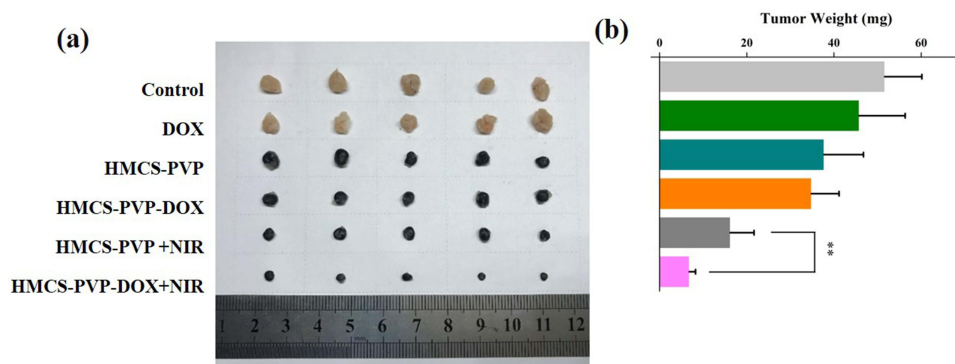


**Figure 7** (a) Photographs and (b) weights of lymph nodes dissected from each group at 16th day after phototherapy treatment (data are means  $\pm$  SD, N=5); \*\* $p < 0.01$ .

## Lymphatic Metastasis Tumor Treatment

Inspired by the PA imaging ability of HMCS-PVP-DOX nanoparticles under laser irradiation and the effect of in vitro tumor suppression assay, we further evaluated their anti-tumor ability on mice with 4T1 sentinel lymphatic metastatic tumors. The 4T1 tumor cells were first injected into the foot pads of mice to induce metastasis to the sentinel lymph nodes and caused lymph node enlargement, and when the lymph nodes became hard masses like green beans, these induced lymphatic metastatic tumor mice were divided into 6 groups ( $n=5$ ), and the groups were as follows: PBS group (control group), DOX group, HMCS-PVP group, HMCS-PVP-DOX group, the HMCS-PVP+Laser group and HMCS-PVP-DOX+Laser group. All groups were administered by footpad injection, followed by laser ( $1064 \text{ nm}$ ,  $0.75 \text{ W cm}^{-2}$ ,  $5 \text{ min}$ ) irradiation of the sentinel lymph node site 1 h after injection. After irradiation, the mice were housed for 16 days and were weighed every 2 days to observe their physiological functions. At the end of the treatment, the mice were executed, and the sentinel lymph nodes were removed from the leg fossa of the mice.

In terms of the weight of the final sentinel lymph nodes in the mice (Figure 7), the HMCS-PVP group and the HMCS-PVP-DOX group showed a good lymphatic enrichment effect on the lymphatic metastases in the mice, which were stained black and remained visible at the lymph nodes after up to 16 days of physiological activity, in contrast to the surrounding tissues or organs. The control group had the most severe lymph node enlargement, compared with the DOX and HMCS-PVP groups, which had almost no anti-tumor ability and tumor weight of 45.7 and 37.7 mg, respectively. This was due to the inability of small molecule chemotherapeutic agents to reach the lymphatic metastases through the lymphatic vessels and the inability of HMCS-PVP to ablate the tumor without NIR laser irradiation.

The tumors in the HMCS-PVP-DOX group were larger than those in the HMCS-PVP+Laser group. This was because the slow release of the drug in HMCS-PVP-DOX. While photothermal could quickly warm up to  $>60^\circ\text{C}$ , indicating that the temperature was high enough to kill the tumor cells in the lymph nodes effectively. For the HMCS-PVP-DOX+Laser group, the growth of lymphatic tumors was significantly inhibited, and only 6.8 mg of tumors remained. The metastatic tumor enlargement almost disappeared, which indicated that the synergistic treatment was effective in inhibiting the growth of metastatic tumors in lymph nodes. The above results indicated that HMCS-PVP-DOX could effectively act on tumors under laser irradiation (HMCS-PVP-DOX+Laser group) resulting in significant inhibition of tumor growth in lymph nodes, showing good potential for reducing the risk of cancer metastasis as well as long-lasting lymphatic tracing.

## Biosafety Evaluation

The biocompatibility of the nanoparticles in vitro was explored. As shown in Figures S2 and S3, the cellular toxicity of the chemotherapeutic drug DOX was obvious, and the survival rate was only 26.8% at a concentration of  $10 \mu\text{g mL}^{-1}$ . Both HMCS-PVP and HMCS-PVP-DOX showed good biocompatibility, and the cell survival rate was still above 80% even at a concentration of  $200 \mu\text{g mL}^{-1}$ . HMCS-PVP, as a carrier for chemotherapeutic drugs, had good biocompatibility after wrapping the apparently toxic DOX, demonstrating its ability to transport chemotherapeutic drugs for subsequent in vivo experiments. On this basis, we further investigated the effect of the addition of photothermal on cytotoxicity by incubating HMCS-PVP and HMCS-PVP-DOX groups for 4 h after addition to cell culture plates, and then irradiating

them with NIR laser (1064 nm, 1 W cm<sup>-2</sup>, 5 min). PVP-DOX+Laser group had a more obvious effect of tumor cell death than both single HMCS-PVP+Laser group and single DOX group, which laid the foundation for the subsequent in vivo treatment experiments.

To further explore the biosafety of HMCS-PVP-DOX in vivo, mice were randomly divided into 3 groups (n=3) and injected with PBS, HMCS-PVP and HMCS-PVP-DOX (50 μL in PBS, HMCS=50 mg mL<sup>-1</sup>). The results were shown in [Figures S4](#) and [S5](#) and [Table S1](#). From the results, it could be seen that the body indexes did not change significantly after administration, indicating that HMCS-PVP-DOX had superior biosafety.

One mouse at the end of the treatment was randomly sacrificed, and heart, liver, spleen, lung, kidney and tumor tissue were removed by dissection and sectioned using hematoxylin–eosin (H&E) staining for histological analysis. From the staining results of H&E ([Figure S6](#)), no inflammation or damage to organs and tissues was found in other mice compared with the control group, demonstrating that HMCS-PVP-DOX was non-toxic and could be used as an efficient and long-lasting lymphatic tracer for clinical applications and treatment of lymphatic metastases.

## Conclusions

In summary, we prepared nanocarbon lymphatic contrast tracers HMCS-PVP-DOX with awesome biocompatibility and exemplary clinical applications. The size of HMCS could be adjusted as necessitated and be fabricated to materialize miscellaneous functions. HMCS-PVP-DOX substantiated an estimable lymphatic targeting capability and salient visual recognition effect. Even more, the PA imaging competency of HMCS-PVP was tremendously vigorous, providing an apparatus for non-invasive detection of lymph node locations and tumor cell metastasis status. Due to the porosity and cavities, HMCS-PVP featured a marvelous drug loading potential. DOX-loaded HMCS-PVP could be used not only for the detection of lymph node metastases, but also for the inhibition of tumor cell growth in lymph nodes in synergy with light and heat, thus reducing the risk of lymphatic metastasis of tumor cells. In vitro and in vivo experiments signified that the HMCS-PVP-DOX with laser irradiation group had a superb ability to stifle the growth of tumor cells. Guided by PA/photothermal imaging signals, HMCS-PVP-DOX enabled precise diagnosis and PTT of lymph node tumors. The experimental results unveiled that HMCS-PVP-DOX could release drugs and consummate synergistic chemotherapy-PTT on metastatic lymph nodes under the stimulation of photothermal heat. On top of that, HMCS-PVP-DOX exhibited terrific stability, biocompatibility and innocuousness, which was conducive to further clinical applications in tumor lymphatic metastasis imaging and treatment.

## Acknowledgments

This work was funded by the National Natural Science Foundation of China (81703021, 81772604) and Shanghai Pujiang Program (2020PJD56).

## Disclosure

There are no competing interests to declare.

## References

1. Siegel RL, Miller KD, Jemal A. Cancer statistics, 2019. *CA Cancer J Clin*. 2019;69(1):7–34. doi:10.3322/caac.21551
2. Riggi N, Aguet M, Stamenkovic I. Cancer metastasis: a reappraisal of its underlying mechanisms and their relevance to treatment. *Annu Rev Pathol*. 2018;13(1):117–140. doi:10.1146/annurev-pathol-020117-044127
3. He Q, Guo S, Qian Z, Chen X. Development of individualized anti-metastasis strategies by engineering nanomedicines. *Chem Soc Rev*. 2015;44(17):6258–6286. doi:10.1039/C4CS00511B
4. Farnsworth RH, Achen MG, Stacker SA. The evolving role of lymphatics in cancer metastasis. *Curr Opin Immunol*. 2018;53:64–73. doi:10.1016/j.coi.2018.04.008
5. Karaman S, Detmar M. Mechanisms of lymphatic metastasis. *J Clin Invest*. 2014;124(3):922–928. doi:10.1172/JCI171606
6. Stacker SA, Caesar C, Baldwin ME, et al. VEGF-D promotes the metastatic spread of tumor cells via the lymphatics. *Nat Med*. 2001;7(2):186–191. doi:10.1038/84635
7. Alitalo K, Tammela T, Petrova TV. Lymphangiogenesis in development and human disease. *Nature*. 2005;438(7070):946–953. doi:10.1038/nature04480
8. Denschlag D, Gabriel B, Mueller-Lantzsch C, et al. Evaluation of patients after extraperitoneal lymph node dissection for cervical cancer. *Gynecol Oncol*. 2005;96(3):658–664. doi:10.1016/j.ygyno.2004.08.053

9. Hirano A, Kamimura M, Ogura K, et al. A comparison of indocyanine green fluorescence imaging plus blue dye and blue dye alone for sentinel node navigation surgery in breast cancer patients. *Ann Surg Oncol*. 2012;19(13):4112–4116. doi:10.1245/s10434-012-2478-0
10. Choi S-B, Kim K-S, Choi J-Y, et al. The prognosis and survival outcome of intrahepatic cholangiocarcinoma following surgical resection: association of lymph node metastasis and lymph node dissection with survival. *Ann Surg Oncol*. 2009;16(11):3048–3056. doi:10.1245/s10434-009-0631-1
11. Upputuri PK, Pramanik M. Recent advances toward preclinical and clinical translation of photoacoustic tomography: a review. *J Biomed Opt*. 2016;22(4):041006–041019. doi:10.1117/1.JBO.22.4.041006
12. El-Sherief AH, Lau CT, Obuchowski NA, et al. Cross-disciplinary analysis of lymph node classification in lung cancer on CT scanning. *Chest*. 2017;151(4):776–785. doi:10.1016/j.chest.2016.09.016
13. Muehe AM, Siedek F, Theruvath AJ, et al. Differentiation of benign and malignant lymph nodes in pediatric patients on ferumoxytol-enhanced Pet/MRI. *Theranostics*. 2020;10(8):3612–3621. doi:10.7150/thno.40606
14. Dias AH, Holm Vendelbo M, Bouchelouche K. Prostate-specific membrane antigen Pet/CT: uptake in lymph nodes with active sarcoidosis. *Clin Nucl Med*. 2017;42(3):e17e176. doi:10.1097/RLU.0000000000001528
15. Saad ZZ, Omorphos S, Michopoulou S, et al. Investigating the role of Spect/CT in dynamic sentinel lymph node biopsy for penile cancers. *Eur J Nucl Med Mol Imaging*. 2017;44(7):1176–1184. doi:10.1007/s00259-017-3636-1
16. Chen Q, Liang C, Wang X, He J, Li Y, Liu Z. An albumin-based theranostic nano-agent for dual-modal imaging guided photothermal therapy to inhibit lymphatic metastasis of cancer post surgery. *Biomaterials*. 2014;35(34):9359362. doi:10.1016/j.biomaterials.2014.07.062
17. Fernandez-Fernandez A, Manchanda R, Lei T, et al. Comparative study of the optical and heat generation properties of Ir820 and indocyanine green. *Mol Imaging*. 2012;11(2):99–113. doi:10.2310/7290.2011.00031
18. Torabi M, Aquino SL, Harisinghani MG. Current concepts in lymph node imaging. *J Nucl Med*. 2004;45(9):1509–1518.
19. Song KH, Kim C, Cobley CM, Xia Y, Wang LV. Near-infrared gold nanocages as a new class of tracers for photoacoustic sentinel lymph node mapping on a rat model. *Nano Lett*. 2009;9(1):183–188. doi:10.1021/nl802746w
20. Yang Z, Tian R, Wu J. Impact of semiconducting perylene diimide nanoparticle size on lymph node mapping and cancer imaging. *ACS Nano*. 2017;11(4):4247–4255. doi:10.1021/acsnano.7b01261
21. Pan D, Cai X, Yalaz C, et al. Photoacoustic sentinel lymph node imaging with self-assembled copper neodecanoate nanoparticles. *ACS Nano*. 2012;6(2):1260–1267. doi:10.1021/nn203895n
22. Kim C, Song KH, Gao F, et al. Sentinel lymph nodes and lymphatic vessels: noninvasive dual-modality in vivo mapping by using indocyanine green in rats—volumetric spectroscopic photoacoustic imaging and planar fluorescence imaging. *Radiology*. 2010;255(2):442–450. doi:10.1148/radiol.10090281
23. Wang S, Cao Y, Zhang Q, et al. New application of old material: Chinese traditional ink for photothermal therapy of metastatic lymph nodes. *ACS Omega*. 2017;2(8):5170–5178. doi:10.1021/acsomega.7b00993
24. Liu X, Chang S, Jiang X, Huang P, Yuan Z. Identifying parathyroid glands with carbon nanoparticle suspension does not help protect parathyroid function in thyroid surgery: a Prospective, Randomized Control Clinical Study. *Surg Innov*. 2016;23(4):381–389. doi:10.1177/1553350615624787
25. Yang F, Jin C, Yang D, et al. Magnetic functionalised carbon nanotubes as drug vehicles for cancer lymph node metastasis treatment. *Eur J Cancer*. 2011;47(12):1873–1882. doi:10.1016/j.ejca.2011.03.018
26. Tian R, H. M, Zhu S, et al. Multiplexed Nir-Ii probes for lymph node-invaded cancer detection and imaging-guided surgery. *Adv Mater*. 2020;32(11):1907361907310.
27. Liu Z, Robinson JT, Tabakman SM, et al. Carbon materials for drug delivery & cancer therapy. *Mater Today*. 2011;14(7–8):316–323. doi:10.1016/S1369-7021(11)70161-4
28. Cousins A, Thompson SK, Wedding AB, et al. Clinical relevance of novel imaging technologies for sentinel lymph node identification and staging. *Biotechnol Adv*. 2014;32(2):269–279. doi:10.1016/j.biotechadv.2013.10.011
29. Zou L, Wang H, He B, et al. Current approaches of photothermal therapy in treating cancer metastasis with nanotherapeutics. *Theranostics*. 2016;6(6):762–772. doi:10.7150/thno.14988
30. He X, Bao X, Cao H. Tumor-penetrating nanotherapeutics loading a near-infrared probe inhibit growth and metastasis of breast cancer. *Adv Funct Mater*. 2015;25(19):2831–2839. doi:10.1002/adfm.201500772
31. Liang C, Diao S, Wang C, et al. Tumor metastasis inhibition by imaging-guided photothermal therapy with single-walled carbon nanotubes. *Adv Mater*. 2014;26(32):5646–5652. doi:10.1002/adma.201401825
32. Zhang W, Song S, Wang H, et al. In vivo irreversible albumin-binding near-infrared dye conjugate as a naked-eye and fluorescence dual-mode imaging agent for lymph node tumor metastasis diagnosis. *Biomaterials*. 2019;217:119279. doi:10.1016/j.biomaterials.2019.119279
33. Rao DA, Forrest ML, Alani AWG, Kwon GS, Robinson JR. Biodegradable Plga Based Nanoparticles for Sustained Regional Lymphatic Drug Delivery. *J Pharm Sci*. 2010;99(4):2018–2031. doi:10.1002/jps.21970
34. Kobayashi H, Kawamoto S, Bernardo M, et al. Delivery of gadolinium-labeled nanoparticles to the sentinel lymph node: comparison of the sentinel node visualization and estimations of intra-nodal gadolinium concentration by the magnetic resonance imaging. *J Control Release*. 2006;111(3):343–351. doi:10.1016/j.jconrel.2005.12.019
35. Cong L, Takeda M, Hamanaka Y. Uniform silica coated fluorescent nanoparticles: synthetic method, improved light stability and application to visualize lymph network tracer. *PLoS One*. 2010;5(10):e13167–13166. doi:10.1371/journal.pone.0013167
36. Johnson L, Charles-Edwards G, Douek M. Nanoparticles in sentinel lymph node assessment in breast cancer. *Cancers*. 2010;2(4):1884–1894.
37. Manolova V, Flace A, Bauer M, et al. Nanoparticles target distinct dendritic cell populations according to their size. *Eur J Immunol*. 2008;38(5):1404–1413. doi:10.1002/eji.200737984
38. Sun J, Li Y, Teng Y, Wang S, Guo J, Wang C. NIR-controlled HSP90 inhibitor release from hollow mesoporous nanocarbon for synergistic tumor photothermal therapy guided by photoacoustic imaging. *Nanoscale*. 2020;12(27):14775–14787. doi:10.1039/D0NR02896G

International Journal of Nanomedicine

Dovepress

## Publish your work in this journal

The International Journal of Nanomedicine is an international, peer-reviewed journal focusing on the application of nanotechnology in diagnostics, therapeutics, and drug delivery systems throughout the biomedical field. This journal is indexed on PubMed Central, MedLine, CAS, SciSearch®, Current Contents®/Clinical Medicine, Journal Citation Reports/Science Edition, EMBase, Scopus and the Elsevier Bibliographic databases. The manuscript management system is completely online and includes a very quick and fair peer-review system, which is all easy to use. Visit <http://www.dovepress.com/testimonials.php> to read real quotes from published authors.

Submit your manuscript here: <https://www.dovepress.com/international-journal-of-nanomedicine-journal>